



ANN modeling for scale-up of green synthesis of iron oxide nanoparticle and its application for decolorization of dye effluent

K. Sathya^a, R. Saravanathamizhan^{a,*}, G. Baskar^b

^aDepartment of Chemical Engineering, A.C. Tech., Anna University, Chennai 600025, India, Tel. +91 44 22359237; email: thamizhan79@rediffmail.com (R. Saravanathamizhan), Tel. +91 44 22359237, email: satyakarunakaran@gmail.com (K. Sathya)

^bDepartment of Bio Technology, St. Joseph's College of Engineering, Chennai 600119, India, Tel. +91 9443678571; email: basg2004@gmail.com (G. Baskar)

Received 23 February 2018; Accepted 9 April 2018

ABSTRACT

Nanomaterials are synthesized in the laboratory scale and converting it to industrial scale is still a challenge. In this work, green synthesis of iron oxide nanoparticle has been carried out using *Coriandrum sativum* leaf extract as a reducing agent, and the experimental operating parameters such as time, temperature, ferric chloride concentration, and stirring speed for the yield of nanoparticles were optimized. Using this laboratory data, an artificial neural network (ANN) model has been used to determine the yield of iron oxide nanoparticle. It is observed from this work that ANN model is a useful tool to scale up the production of iron oxide nanoparticle from lab-scale to industrial-scale application. The neural network configuration of one hidden layer with six neurons (4-6-1) matches well with the experimental values. Further the photocatalytic decolorization of direct red dye wastewater has been reported using the green-synthesized iron oxide nanoparticle. The iron oxide nanoparticle showed maximum decolorization efficiency of 87% at 10 mg L⁻¹ concentration of direct red dye.

Keywords: Artificial neural network model; *Coriandrum sativum* leaf extract; Green synthesis; Iron oxide nanoparticle; Decolorization

1. Introduction

The particles ranging from 1 to 100 nm in size are called nanoparticles. Due to their size and surface area, it has totally different characteristics and properties [1]. Nanomaterials are widely used in many fields such as biomedicine [2], cosmetics [3], and electronics [4]; in food industry as antimicrobial and food preservative agent [5]; and in environment for dye removal and heavy metal removal [6].

Different methods such as chemical [7], physical [8], and biological [9] are used for the synthesis of nanomaterials. However, the usage of toxic reducing agent, high cost of production, energy requirement, etc. [10] adds to the disadvantage of chemical and physical method. Hence, the biological

method acts as an eco-friendly alternative for the above methods. The biological methods include usage of microbes [11] and plant sources [12–15] for the synthesis of nanomaterials. The plant-mediated synthesis is considered to be more advantageous over other methods because microbe-mediated synthesis consumes time and requires aseptic conditions [16].

There are more number of works reported earlier based on the plant-mediated synthesis of metal oxide nanoparticles. For example, ZnO synthesized from leaf extracts of *Anisochilus carnosus* [17]; *Plectranthus amboinicus* [18], and *Vitex negundo* [19]; iron oxide nanomaterials synthesized from soybean sprouts [20]; *Syzygium cumini* seed extract [21]; *Ocimum sanctum* leaf extract [22]; plantain peel extract [23]; and palladium nanoparticles from *Terminalia chebula* leaf extract [24]. Among the nanomaterials synthesized, magnetic nanoparticles play a

* Corresponding author.

significant role in targeted drug delivery and treatment, photocatalytic property, magnetic resonance imaging, and computer tomography imaging due to their unique magnetic and catalytic properties. Photocatalytic activity of iron nanoparticles synthesized from *Amaranthus dubius* leaf extract was reported by Harshiny et al. [25]. The effect of process parameters, such as pH, temperature, concentration, and time on antioxidant property and synthesis process has been studied, and the author reported that green-synthesized nanoparticle is spherical in shape with cubic phase structure and the diameter ranges from 43 to 220 nm. It shows better methyl orange decolorization efficiency of 81% than that in the nanoparticle prepared from chemical method. Shahwan et al. [26] synthesized iron nanoparticles from green tea leaf extract. They compared the degradation efficiency of chemical and green-synthesized nanoparticles using cationic and anionic dyes. They have reported that green-synthesized iron nanoparticle shows better degradation efficiency of 100% at 10 mg L⁻¹ concentration compared with iron nanoparticle synthesized by chemical method. The hybrid technique for synthesis of iron nanoparticle from eucalyptus leaf extract and encapsulation in chitosan beads was reported by Martinez-Cabanas et al. [27]. The authors have reported that the synthesized magnetic hybrid beads were effective in the removal of arsenic with short equilibrium time and good adsorption capacity at normal pH.

Though the biological- and plant-mediated synthesis of nanomaterials is considered to be booming in lab scale, it is essential to scale up the process to industry level. For this purpose, artificial neural network (ANN) modeling has been used to scale up the process to industrial scale. ANN has been successfully used to solve environmental engineering problems. ANNs have wide range of applications such as speech recognition, fault detection and diagnosis, pollutant-removal studies, etc. Different applications of ANN modeling have been reported in the previous literatures. The performance of chemical oxygen demand removal in the batch reactor was predicted using ANN by Basha et al. [28]; removal of chromium from polluted solutions by electrocoagulation was modeled using ANN [29]; ANNs were used to predict methyl orange dye adsorption on polyaniline nano-adsorbent [30]; the process optimization and modeling for pollutant removal from water using response surface methodology (RSM) and artificial neural network-genetic algorithm by Sweta et al. [31]; and Tahani et al. [32] used the ANN modeling for studying the thermal conductivity of graphene oxide nanoplatelets/deionized water nanofluids. They have found that the ANN model can predict the thermal behavior of the nanofluid precisely. The electrooxidation of simulated wastewater using continuous stirred tank electrochemical reactor was done using RSM and ANN modeling by Saravanathamizhan et al. [33]. The authors reported that ANN model results were in good agreement with experimental values.

Modeling of nanoparticle synthesis has also been reported in the literature. Sakthivel and Pitchumani [34] studied the effect of nanoparticle size using RSM. Shabanzadeh et al. [35] predicted nanoparticle size synthesized using chemical reduction method using ANN modeling. It was found that ANN modeling is helpful in predicting the results [36–39]. The lab-scale production is very less, hence in this work, green synthesis of iron oxide nanomaterial has been attempted to scale up to industrial level using ANN modeling.

1.1. Artificial neural networks

The objective of a neural network is to compute output values from input values by some internal calculations. ANNs are biologically inspired computer programs designed to simulate the way in which the human brain processes information. ANNs gather their knowledge by detecting the patterns and relationships in data, and learn (or train) from experience and not from programming.

The processing elements of the ANNs are known as “neurons” that are the processing elements of ANNs connected to each other and function concurrently [40,41]. The ANN includes three layers—input layer, one or more hidden layer, and output layer. The information received by a neuron from the other neuron is processed, and the signal is passed to the consecutive neurons. These neurons are connected with coefficients (weights), which form the neural structure which has been organized in layers. Connecting the neurons in a network is important for neural network modeling. Each neuron has weighted inputs, transfer function, and one output. The transfer functions of neurons, the learning rule, and the architecture determine the behavior of a neural network [42]. The activation of the neuron is based on the weighed sum of the inputs. Single output of the neuron is obtained by giving the activation signal through transfer function which introduces nonlinearity to the network [43]. The error in predictions is minimized until interunit connections are optimized till it reaches accuracy, and new input information is given to predict the output. Different types of neural networks have been reported earlier and new types of networks are developed frequently, but they can be described by the transfer functions of their neurons by the learning rule and connection formula.

The backpropagation (BP) neural network is widely used for the modeling in order to minimize the error. This algorithm is used in layered feed-forward ANNs [44]. In this network, signals are send forward then the errors signals are propagated backwards. The network receives input in the input layer, the internal calculation is done in the hidden layers by neurons, and output network by output layer. The idea of the BP algorithm is to reduce this error, until the ANN learns the training data. The training begins with random weights, and the goal is to adjust them so that the error will be minimal.

There are 14 training function available in the MATLAB 7 toolbox. Trainlm and trainscg functions are commonly used training functions, and tan-sigmoid (tansig), log-sigmoidal (logsig), and linear (purelin) functions are commonly used transfer functions in the ANN modeling.

The training function and transfer functions trainlm and tansig are chosen, respectively, for this work based on trial and error method. All inputs and outputs were linearly normalized before entering in ANN, using the following equation [29]:

$$A_i = \frac{(X_i - X_{\min})}{(X_{\max} - X_{\min})}(r_{\max} - r_{\min}) + r_{\min} \quad (1)$$

where X_i is input or output of the network; A_i is the normalized value of X_i ; X_{\min} and X_{\max} are extreme values of X_i ;

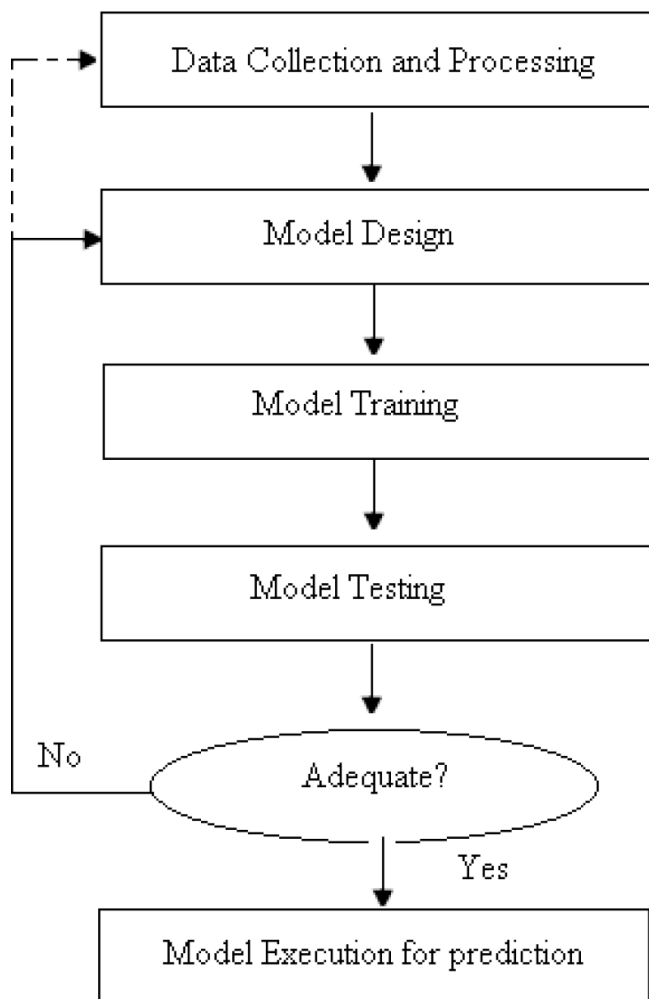


Fig. 1. Flow chart for ANN modeling.

and r_{\min} and r_{\max} define the limits of the range where X_i is scaled. In this work, input and output data are normalized between 0.1 and 0.9. After modeling, results were converted to original state.

The various steps in developing a neural network models are shown in the flowchart (Fig. 1). The first step in the neural network modeling is data collection. For the various input variables, the experimental data have been collected and fed as an input to the neural network. The entire set of data is split in to three categories, namely training, testing, and validation. The training set is the largest set and is used by neural network to learn patterns present in the data. The testing set is used to evaluate the generalization ability of a clearly trained network. A final check on the performance of the trained network is made using the validation set.

2. Materials and methods

2.1. Chemicals

Ferric chloride, hydrochloric acid, sodium hydroxide pellets, 2,2-diphenyl-1-picrylhydrazyl, and ethanol were procured from SRL Pvt. Ltd., India, and were used without any further purification.

2.2. Preparation of *Coriandrum sativum* leaf extract

Fresh leaves were collected and washed several times by using distilled water. The leaf extract was prepared by taking 30 g of finely cut leaves and then homogenized using blender, centrifuged and the supernatant was collected, made up to 100 mL by distilled water, and stored at 4°C for further use.

2.3. Synthesis of iron oxide nanoparticles

A total of 50 mL of freshly prepared homogenized leaf extract was added dropwise to 50 mL of 0.5 M ferric chloride solution under continuous stirring. The pH of the solution was adjusted using 0.1 N HCl and 0.1 N NaOH. The change in color of the solution and formation of black precipitate indicates the synthesis of iron oxide nanoparticle. The iron oxide nanoparticle precipitate formed was centrifuged, dried, and stored for characterization. The formation of nanoparticle was observed by UV spectra. The details about instrumentation and characterization results were presented in our previous paper [45]. Band gap energy of the nanoparticle is estimated using ultraviolet-diffuse reflection spectroscopy. The band gap has been calculated using the formula ($E = 1240/\lambda$ where, λ is the wave length) and found to be 2.26 eV.

2.4. Feed-forward BPNN model

In the feed-forward backpropagation neural network model (BPNN), signals are sent forward then the errors signals are propagated backward, hence the error get minimized. Generally, ANN requires three types of layers: input, hidden, and output layer. A typical neural network configuration is shown in Fig. 2. The input is given to the input layer, output layer is the response, and the hidden layer is the feature predictor of the model. The hidden layer contains the neurons. The hidden layer and number of neuron selection for the model were done by trial and error method. All these calculation for this study has been carried out using Neural Network Toolbox of MATLAB 7. The training is repeated until the convergence is reached by changing the number of neurons and hidden layers. Each network is tested for its ability in predicting the performance of the process by comparing prediction with experimental observations. Sum of squared error (SSE), mean squared error (MSE), and mean absolute error (MAE) are expressed as follows [46]:

$$SSE = \sum_{i=1}^N (t_i - a_i)^2 \quad (2)$$

$$MSE = \frac{1}{N} \sum_{i=1}^N (t_i - a_i)^2 \quad (3)$$

$$MAE = \frac{1}{N} \sum_{i=1}^N |t_i - a_i| \quad (4)$$

where N is the total number of data, t_i is the target value, and a_i is the network output value.

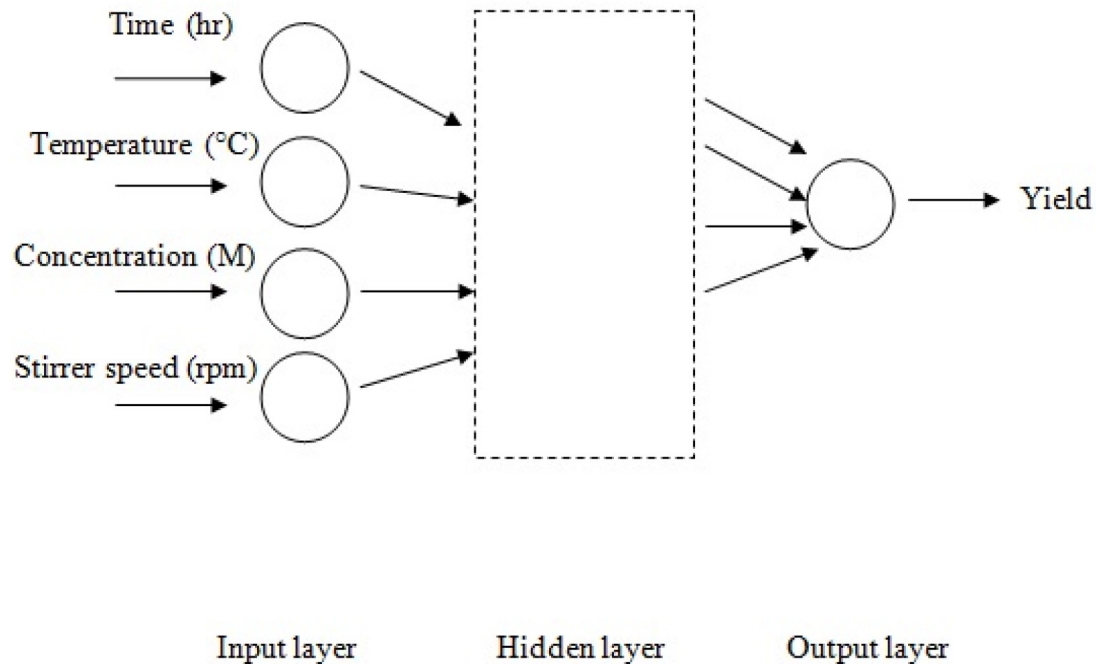


Fig. 2. The typical neural network architecture for modeling.

2.5. Photocatalytic activity

The photocatalytic activity of the iron oxide nanoparticle prepared was performed by decolorization of direct red dye solution under UV irradiation. The photocatalytic apparatus consists of three 300 W xenon lamps, magnetic stirrer, and cooling fans. The magnetic stirrer is used for maintaining uniform mixing, and the cooling fans are provided to maintain temperature. A total of 0.1 g of nanoparticle was added to 50 mL of 10, 20, 30, 40, and 50 mg L⁻¹ aqueous dye solution and kept in the chamber. The samples were collected at the end of 2 h of time and analyzed using a UV-visible spectrophotometer with a wavelength range of 200–900 nm. The decolorization of direct red dye is calculated using the following formula:

$$\text{Color removal \%} = \frac{C_o - C_t}{C_o} \times 100 \quad (5)$$

where C_o and C_t are the initial concentration and the concentration after time t of direct red dye solution, respectively.

2.6. Mechanism of decolorization and its influencing factors

In the photocatalytic oxidation using iron oxide nanoparticle, the light illumination produces excited high-energy states of electron and hole pairs (e^-/h^+). Part of the photo-generated carriers recombine and migrate to the surface of particles, where the holes act as oxidizing agent and the electrons as powerful reductants, which lead to complete mineralization of the dyes. The HO^\bullet radicals formed are extremely powerful oxidizing agents that nonselectively attack the adsorbed organic molecules or those close to the catalyst surface, resulting in the decolorization of dye effluent.

3. Result and discussions

3.1. Effect of operating parameters

The effect of operating parameters such as time, salt concentration, temperature, and string speed on percentage yield of iron oxide nanoparticle are presented in Figs. 3–6. The effect of time for 500 and 800 rpm on iron oxide nanoparticle yield is shown in Fig. 3. It is observed from Fig. 3 that the yield increases with increase in time and stirring speed. The formation of nuclei for nanoparticle is increased with increase in time and stirring speed which results the increase of nanoparticle yield. The effect of temperature for 500 and 800 rpm on iron oxide nanoparticle yield is shown in Fig. 4. It is observed from figure that the yield decreases with increase in temperature. The maximum yield is obtained just above room temperature. The higher temperature affects the yield of nanoparticle, size, and structure. At higher temperature, the solution evaporates rapidly which leads to decrease in the yield of nanoparticle, further at optimum temperature only the reduction iron salt to form iron oxide nanoparticle will be more. The salt concentration also plays an important role in the yield of the nanoparticle. The effect of salt concentration for 500 and 800 rpm on iron oxide nanoparticle yield is shown in Fig. 5. Increase in salt concentration leads to increase in the yield. Maximum yield is obtained for 0.5 M salt concentration. This is due to the availability of salt to be reduced by plant extract. Fig. 6 shows that effect of stirring speed on nanoparticle yield for 0.1 and 0.5 M salt concentration. The particle size reduces with the increase in stirring speed; there will be formation of small nuclei during mixing because of rapid nucleation process which increases the yield. These results are in good agreement with the results obtained by Babou-Kammoe et al. [47] and Agnihotri et al. [48].

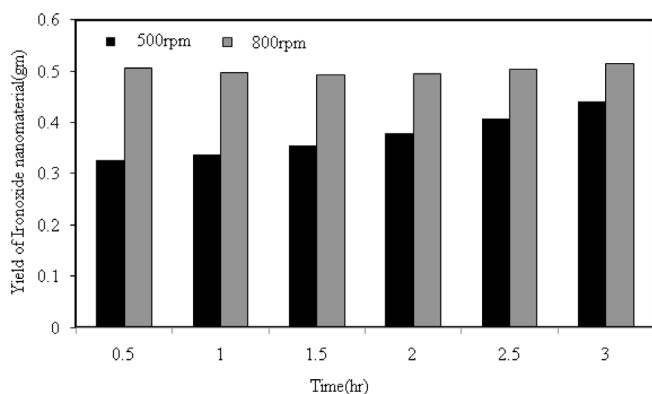


Fig. 3. Effect of time on yield of iron oxide nanoparticle (salt concentration, 0.5 M and temperature, 30°C).

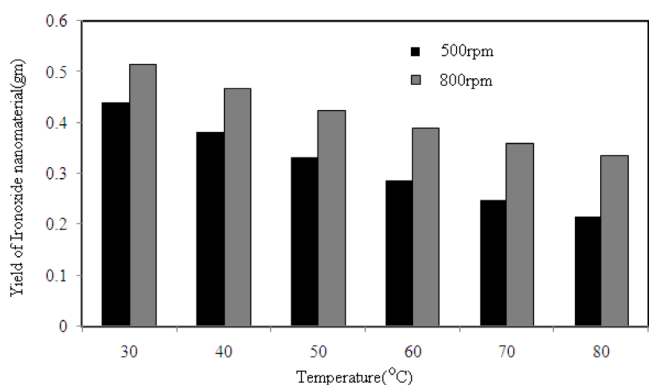


Fig. 4. Effect of temperature on yield of iron oxide nanoparticle (salt concentration, 0.5 M and time, 3 h).

3.2. Simulation and scale-up using ANN

In this work, around 200 data were used. The data split in to three sets for training, testing, and validation. These data were collected for different combination of operating parameters, such as time, salt concentration, stirring speed, and temperature. Various neural networks were selected and trained for the trial and error method and checked with the available data. The number of hidden layer and neurons selected for this study is shown in Table 1. The trial started with the case of single hidden layer. The number of neurons in the hidden layer is varied for 2, 4, 5, 6, 7, 8, and 9; the corresponding networks are notated N1, N2, N3, N4, N5, N6, N7, and N8, respectively. The test results along with their performance terms SSE, MSE, and MAE are presented in Table 1. Experimental and simulated results for the different time, temperature, concentration, and stirring speed are presented in Table 2, for the various network configurations (N1, N2, N3, N4, N5, N6, N7, and N8). It can be observed from tables that one hidden layer network with the 4-6-1 configuration show less SSE, MSE, and MAE value.

3.3. Decolorization of direct red dye

The photocatalytic degradation of direct dye wastewater using the iron oxide nanocatalyst is shown in Fig. 7. It is observed from the figure that the percentage decolorization decreases with increase in dye concentration. This is due to that the amount of catalyst for the constant light source at

Table 1
Configurations of the neural networks studied

BPNN abbreviation	Configuration	SSE	MSE	MAE
N1	4-2-1	0.66	0.0247	0.1283
N2	4-3-1	1.06	0.0393	0.1600
N3	4-4-1	0.25	0.0094	0.0795
N4	4-5-1	0.23	0.0085	0.0730
N5	4-6-1	0.20	0.0075	0.0723
N6	4-7-1	0.66	0.0246	0.118
N7	4-8-1	0.21	0.0079	0.0715
N8	4-9-1	0.81	0.0299	0.141

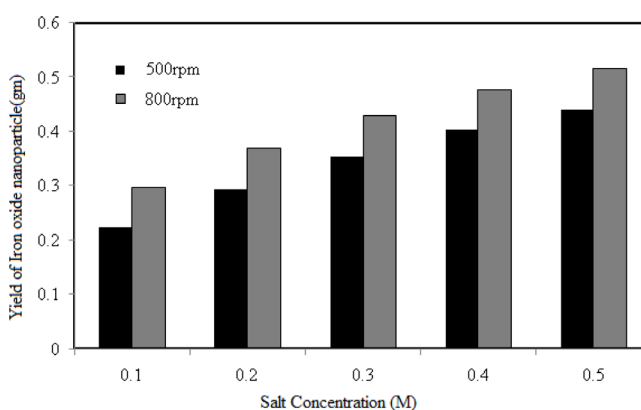


Fig. 5. Effect of salt concentration on yield of iron oxide nanoparticle (time, 3 h and temperature, 30°C).

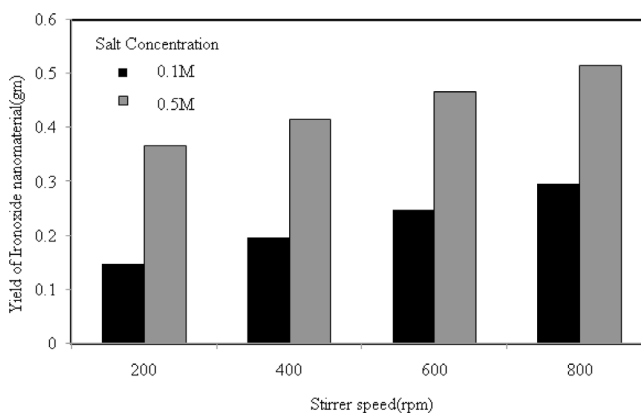


Fig. 6. Effect of stirring rate on yield of iron oxide nanoparticle (time, 3 h and temperature, 30°C).

higher concentration is difficult to decolorize the dye. The maximum decolorization of 87% is achieved for the present condition.

4. Conclusions

Iron oxide nanoparticle has been synthesized using *Coriandrum sativum* leaf extract as a reducing agent. Effect of operating parameters, such as time, ferric chloride concentration, stirring speed, and temperature on the yield of iron oxide nanoparticles has been studied. The ANN modeling has been attempted to model and scale up the yield

Table 2
Experimental and predicted values of green synthesis of iron oxide nanoparticle yield

Si. No.	Time (h)	Temperature (°C)	Concentration (M)	Stirrer speed (rpm)	Iron oxide nanoparticle yield (g)								
					Experimental values	Predicted values							
						N1	N2	N3	N4	N5	N6	N7	N8
1	1	30	0.3	500	0.34	0.14	0.1	0.24	0.19	0.22	0	0.22	0.4
2	1	80	0.3	500	0.24	0.3	0.3	0.14	0.12	0.28	0.05	0.19	0.5
3	1	55	0.1	500	0.27	0.17	0.1	0.12	0.24	0.25	0.23	0.17	0.5
4	1	55	0.5	500	0.22	0.28	0.3	0.25	0.05	0.26	0.25	0.24	0.5
5	1	55	0.3	200	0.09	0.28	0.32	0.16	0.02	0.19	0.17	0.16	0.28
6	1	55	0.3	800	0.45	0.17	0.06	0.23	0.28	0.31	0.13	0.25	0.5
7	2	55	0.1	200	0.08	0.26	0.28	0.17	0.22	0.18	0.32	0.19	0.06
8	2	55	0.5	200	0.11	0.33	0.36	0.28	0.01	0.2	0.13	0.25	0.06
9	2	55	0.1	800	0.36	0.14	0.01	0.24	0.36	0.3	0.41	0.27	0.5
10	2	55	0.5	800	0.39	0.26	0.23	0.32	0.3	0.32	0.16	0.31	0.5
11	2	30	0.3	200	0.22	0.24	0.28	0.27	0.16	0.15	0.17	0.23	0.02
12	2	80	0.3	200	0.06	0.34	0.36	0.19	0.08	0.23	0.13	0.21	0.09
13	2	30	0.3	800	0.45	0.11	0.02	0.31	0.35	0.29	0.34	0.3	0.36
14	2	80	0.3	800	0.38	0.28	0.24	0.25	0.32	0.33	0.32	0.28	0.5
15	2	30	0.1	500	0.25	0.11	0.02	0.25	0.33	0.22	0.38	0.25	0.1
16	2	80	0.1	500	0.24	0.28	0.26	0.16	0.3	0.28	0.36	0.22	0.49
17	2	30	0.5	500	0.38	0.24	0.26	0.33	0.21	0.24	0.05	0.29	0.07
18	2	80	0.5	500	0.16	0.34	0.36	0.27	0.15	0.29	0.01	0.27	0.35
19	2	55	0.3	500	0.26	0.26	0.26	0.26	0.26	0.26	0.26	0.26	0.26
20	3	30	0.3	500	0.35	0.21	0.21	0.33	0.34	0.24	0.4	0.31	0
21	3	80	0.3	500	0.23	0.33	0.35	0.28	0.31	0.29	0.38	0.29	0.08
22	3	55	0.1	500	0.19	0.24	0.21	0.27	0.35	0.26	0.42	0.28	0.06
23	3	55	0.5	500	0.31	0.32	0.34	0.34	0.28	0.27	0.28	0.32	0.05
24	3	55	0.3	200	0.18	0.32	0.35	0.29	0.24	0.2	0.34	0.27	0.14
25	3	55	0.3	800	0.37	0.24	0.18	0.33	0.36	0.31	0.41	0.33	0.24

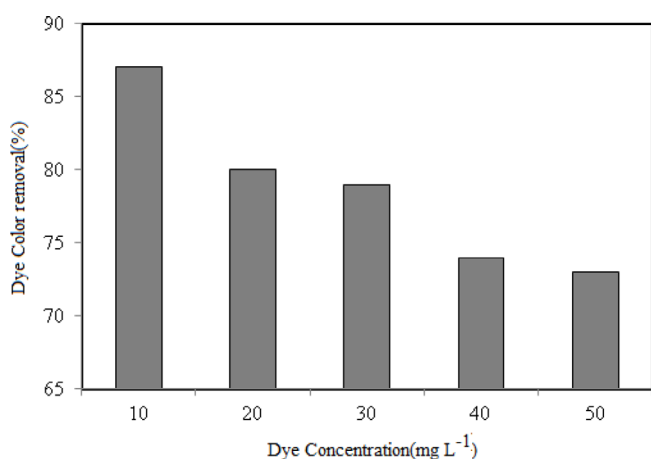


Fig. 7. Photocatalytic decolorization of direct red dye using iron oxide nanoparticle (time, 2 h and iron oxide dosage, 0.1 g).

of the nanoparticle. The configuration of one hidden layer with six neurons (4-6-1) matches well with the experimental values. It is observed from the present investigation that ANN model is a useful tool to scale up the production of iron oxide nanoparticle from lab-scale to industrial-scale application. The photocatalytic decolorization of direct red dye

wastewater has been reported using the green-synthesized iron oxide nanoparticle. It is observed that maximum decolorization efficiency of 87% was achieved at 10 mg L⁻¹ concentration of direct red dye.

5. Acknowledgment

Sathya Karunakaran is thankful to Anna University, Chennai, for Anna Centenary Research Fellowship to carry out the research work.

References

- [1] S. Panigrahi, S. Kundu, S.K. Ghosh, S. Nath, T. Pal, General method of synthesis for metal nanoparticles, *J. Nanopart. Res.*, 6 (2004) 411–414.
- [2] K.G. Ajay, G. Mona, Synthesis and surface engineering of iron oxide nanoparticles for biomedical applications, *Biomaterials*, 26 (2005) 3995–4021.
- [3] L.S. Ana, M.O. Riansares, S.L. Jon, C. Carmen, Nanoparticles: a global vision. Characterization, separation, and quantification methods. Potential environmental and health impact, *Anal. Methods*, 6 (2014) 38–56.
- [4] F. Huilong, P. Zhiwei, L. Lei, Y. Yang, L. Wei, L.G.S. Errol, F. Xiujun, M.T. James, Preparation of carbon-coated iron oxide nanoparticles dispersed on graphene sheets and applications as advanced anode materials for lithium-ion batteries, *Nano Res.*, 7 (2014) 502–510.

- [5] Z. Luksiene, 16—Nanoparticles and their potential application as antimicrobials in the food industry, Elsevier, Amsterdam, 2017, pp. 567–601.
- [6] L. Mohammed, H.G. Gomaa, D. Ragab, J. Zhu, Magnetic nanoparticles for environmental and biomedical applications: a review, *Particuology*, 30 (2017) 1–14.
- [7] Y. Sun, Y. Yin, B.T. Mayers, T. Herricks, Y. Xia, Uniform silver nanowires synthesis by reducing AgNO₃ with ethylene glycol in the presence of seeds and poly(vinyl pyrrolidone), *Chem. Mater.*, 14 (2002) 4736–4745.
- [8] D. Tonti, M. Chergui, Photochemically grown silver nanoparticles with wavelength-controlled size and shape, *Nano Lett.*, 3 (2003) 1565–1568.
- [9] P.R. Swami, R. Selvakannan, M. Sastry, One-step synthesis of ordered two-dimensional assemblies of silver nanoparticles by the spontaneous reduction of silver ions by pentadecylphenol Langmuir monolayers, *J. Phys. Chem. B*, 108 (2004) 19269–19275.
- [10] H. Deepika, L. Jacob, N.N. Rajender, A greener synthesis of core (Fe, Cu)-shell (Au, Pt, Pd, and Ag) nanocrystals using aqueous vitamin C, *ACS Sustainable Chem. Eng.*, 1 (2013) 703–712.
- [11] T. Klaus, R. Joerger, E. Olsson, C.G. Granqvist, Silver-based crystalline nanoparticles, microbially fabricated, *Proc. Natl. Acad. Sci. U.S.A.*, 96 (1999) 13611–13614.
- [12] Y. Konishi, T. Uruga, Bioreductive deposition of platinum nanoparticles on the bacterium *Shewanella algae*, *J. Biotechnol.*, 128 (2007) 648–653.
- [13] S.S. Shankar, A. Ahmed, B. Akkamwar, M. Sastry, A. Rai, A. Singh, Biological synthesis of triangular gold nanoprisms, *Nature*, 3 (2004) 482.
- [14] N. Ahmad, S. Sharma, V.N. Singh, S.F. Shamsi, A. Fatma, B.R. Mehta, Biosynthesis of silver nanoparticles from *Desmodium triflorum*: a novel approach towards weed utilization, *Biotechnol. 1Res. Int.*, 454090 (2011) 1–8.
- [15] S. Roy, T.K. Das, Plant mediated green synthesis of silver nanoparticles—a review, *Int J. Plant Biol. Res.*, 3 (2015) 1044.
- [16] T.X. Fan, S.K. Chow, D. Zhang, Biomorphic mineralization: from biology to materials, *Prog. Mater. Sci.*, 54 (2009) 542–659.
- [17] M. Anbuvarnan, M. Ramesh, G. Viruthagiri, N. Shanmugam, N. Kannadasan, *Anisochilus carnosus* leaf extract mediated synthesis of zinc oxide nanoparticles for antibacterial and photocatalytic activities, *Mater. Sci. Semicond. Process.*, 39 (2015) 621–628.
- [18] L. Fu, Z. Fu, *Plectranthus amboinicus* leaf extract—assisted biosynthesis of ZnO nanoparticles and their photocatalytic activity, *Ceram. Int.*, 41 (2015) 2492–2496.
- [19] S. Ambika, M. Sundrarajan, Antibacterial behaviour of *Vitex negundo* extract assisted ZnO nanoparticles against pathogenic bacteria, *J. Photochem. Photobiol., B*, 146 (2015) 52–57.
- [20] Y. Cai, Y. Shen, A. Xie, S. Li, X. Wang, Green synthesis of soyabean sprouts-mediated superparamagnetic Fe₃O₄ nanoparticles, *J. Magn. Magn. Mater.*, 322 (2010) 2938–2943.
- [21] S. Venkateswarlu, B. Natesh Kumar, C.H. Prasad, P. Venkateswarlu, N.V.V. Jyothi, Bio-inspired green synthesis of Fe₃O₄ spherical magnetic nanoparticles using *Syzygium cumini* seed extract, *Physica B*, 449 (2014) 67–71.
- [22] M.G. Balamurugan, S. Mohanraj, S. Kodhaiyolii, V. Pugalenth, *Ocimum sanctum* leaf extract mediated green synthesis of iron oxide nanoparticles: spectroscopic and microscopic studies, *J. Chem. Pharmacol. Sci.*, 4 (2014) 201–204.
- [23] S. Venkateswarlu, Y.S. Rao, T. Balaji, B. Prathima, N.V.V. Jyothi, Biogenic synthesis of Fe₃O₄ magnetic nanoparticles using plantain peel extract, *Mater. Lett.*, 100 (2013) 241–244.
- [24] K. Mohan Kumar, B. Kumar Mandal, K. Siva Kumar, P. Sreedhara Reddy, B. Sreedhar, Biobased green method to synthesise palladium and iron nanoparticles using *Terminalia chebula* aqueous extract, *Spectrochim Acta, Part A*, 102 (2013) 128–133.
- [25] M. Harshiny, C. Nivedhini Iswarya, M. Matheswaran, Biogenic synthesis of iron nanoparticles using *Amaranthus dubius* leaf extract as a reducing agent, *Powder Technol.*, 286 (2015) 744–749.
- [26] T. Shahwan, S. Abu Sirriah, M. Nairat, E. Boyac, A.E. Eroglub, T.B. Scott, K.R. Hallam, Green synthesis of iron nanoparticles and their application as a Fenton-like catalyst for the degradation of aqueous cationic and anionic dyes, *Chem. Eng. J.*, 172 (2011) 258–266.
- [27] M. Martinez-Cabanas, M. Lopez-Garcia, L. Barriada, R. Herrero, E. Sastre de Vicente, Green synthesis of iron oxide nanoparticles. Development of magnetic hybrid materials for efficient As(V) removal, *Chem. Eng. J.*, 301 (2016) 83–91.
- [28] P. Manokaran, R. Saravanathamizhan, C. Ahmed Basha, T. Kannadasan, Feed-forward back-propagation neural network for the electro-oxidation of distillery effluent, *Chem. Eng. Commun.*, 201 (2014) 1404–1416.
- [29] S. Aber, A.R. Amani-Ghadim, V. Mirzajani, Removal of Cr(VI) from polluted solutions by electrocoagulation: modeling of experimental results using artificial neural network, *J. Hazard. Mater.*, 171 (2009) 484–490.
- [30] M. Tanzifi, S.H. Hosseini, A. Dehghani Kiadehi, M. Olazar, K. Karimipour, R. Rezaeiemehr, I. Ali, Artificial neural network optimization for methyl orange adsorption onto polyaniline nano-adsorbent: kinetic, isotherm and thermodynamic studies, *J. Mol. Liq.*, 244 (2017) 189–200.
- [31] M. Sweta, S. Yogendra, V. Devendra Kumar, H. Syed Hadi Hasan, Synthesis of CuO nanoparticles through green route using *Citrus limon* juice and its application as nanosorbent for Cr(VI) remediation: process optimization with RSM and ANN-GA based model, *Process Saf. Environ. Prot.*, 96 (2015) 156–166.
- [32] M. Tahani, M. Vakili, S. Khosrojerdi, Experimental evaluation and ANN modeling of thermal conductivity of graphene oxide nanoplatelets/deionized water nanofluid, *Int. Commun. Heat Mass Transfer*, 76 (2016) 358–365.
- [33] R. Saravanathamizhan, K. Harsha Vardhan, D. Gnana Prakash, N. Balasubramanian, RSM and ANN modeling for electro-oxidation of simulated wastewater using CSTER, *Desal. Wat. Treat.*, 55 (2014) 1445–1452.
- [34] S. Sakthivel, B. Pitchumani, Optimization of operating variables for production of nanoparticles using response surface modeling, *Chem. Eng. Commun.*, 200 (2013) 289–304.
- [35] P. Shabanzadeh, R. Yusof, K. Shameli, Neural network modeling for prediction size of silver nanoparticles in montmorillonite/starch synthesis by chemical reduction method, *Dig. J. Nanomater. Biostruct.*, 9 (2014) 1699–1711.
- [36] F. Zheng, G. Zheng, A.G. Deaciu, C.G. Zhan, L.P. Dwoskin, P.A. Crooks, Computational neural network analysis of the affinity of lobeline and tetrabenazine analogs for the vesicular monoamine transporter-2, *Med. Chem.*, 15 (2007) 2975–2992.
- [37] B. Louis, V.K. Agrawal, P.V. Khadikar, Prediction of intrinsic solubility of generic drugs using MLR, ANN and SVM analyses, *Eur. J. Med. Chem.*, 45 (2010) 4018–4025.
- [38] M.H. Fatemi, A. Heidari, M. Ghorbanzade, Prediction of aqueous solubility of drug-like compounds by using an artificial neural network and least-squares support vector machine, *Bull. Chem. Soc. Jpn.*, 83 (2010) 1338–1345.
- [39] K.M. Honório, E.F. de Lima, M.G. Quiles, R.A.F. Romero, F.A. Molfetta, A.B.F. Da-silva, Artificial neural networks and the study of the psychoactivity of cannabinoid compounds, *Chem. Biol. Drug Des.*, 75 (2010) 632–640.
- [40] M. Uysala, H. Tanyildizi, Estimation of compressive strength of self-compacting concrete containing polypropylene fiber and mineral additives exposed to high temperature using artificial neural network, *Constr. Build. Mater.*, 27 (2012) 404–414.
- [41] M. Yurdakula, H. Akdas, Modeling uniaxial compressive strength of building stones using non-destructive test results as neural networks input parameters, *Constr. Build. Mater.*, 47 (2013) 1009–1010.
- [42] F. Xiao, S.N. Amirhanian, C. Huang, Prediction of fatigue life of rubberized asphalt concrete mixtures containing reclaimed asphalt pavement using artificial neural networks, *J. Mater. Civil Eng.*, 21 (2009) 253–261.
- [43] L. Bal, F. Buyle-Bodin, Artificial neural network for predicting drying shrinkage of concrete, *Constr. Build. Mater.*, 38 (2013) 248–254.
- [44] P. Cachim, Using artificial neural networks for calculation of temperatures in timber under fire loading, *Constr. Build. Mater.*, 25 (2011) 4175–4180.

- [45] K. Sathya, R. Saravanathamizhan, G. Baskar, Ultrasound assisted phytosynthesis of iron oxide nanoparticle, *Ultrason. Sonochem.*, 39 (2017) 446–451.
- [46] A.M. Zenoos, F.Z. Ashtiani, R. Ranjbar, F. Nikbakht, O. Bolouri, Comparison of different artificial neural network architectures in modeling of *Chlorella* sp. flocculation, *Prep. Biochem. Biotechnol.*, 47 (2017) 570–577.
- [47] R. Babou-Kammoe, S. Hamoudi, F. Larachi, K. Belkacemi, Synthesis of CaCO₃ nanoparticles by controlled precipitation of saturated carbonate and calcium nitrate aqueous solutions, *Can. J. Chem. Eng.*, 90 (2012) 26–33.
- [48] R. Agnihotri, S.K. Mahuli, S.S. Chauk, L.-S. Fan, Influence of surface modifiers on the structure of precipitated calcium carbonate, *Ind. Eng. Chem. Res.*, 38 (1999) 2283–2291.